

# Layout optimization of steel reinforcement in concrete structure using a truss-continuum model

Anbang CHEN<sup>a</sup>, Xiaoshan LIN<sup>a</sup>, Zi-Long ZHAO<sup>b</sup>, Yi Min XIE<sup>a\*</sup>

<sup>a</sup> Centre for Innovative Structures and Materials, School of Engineering, RMIT University, Melbourne 3001, Australia

<sup>b</sup> Institute of Solid Mechanics, School of Aeronautic Science and Engineering, Beihang University, Beijing 100191, China

\*Corresponding author. E-mail: mike.xie@rmit.edu.au

© The Author(s) 2023. This article is published with open access at link.springer.com and journal.hep.com.cn

**ABSTRACT** Owing to advancement in advanced manufacturing technology, the reinforcement design of concrete structures has become an important topic in structural engineering. Based on bi-directional evolutionary structural optimization (BESO), a new approach is developed in this study to optimize the reinforcement layout in steel-reinforced concrete (SRC) structures. This approach combines a minimum compliance objective function with a hybrid truss-continuum model. Furthermore, a modified bi-directional evolutionary structural optimization (M-BESO) method is proposed to control the level of tensile stress in concrete. To fully utilize the tensile strength of steel and the compressive strength of concrete, the optimization sensitivity of steel in a concrete–steel composite is integrated with the average normal stress of a neighboring concrete. To demonstrate the effectiveness of the proposed procedures, reinforcement layout optimizations of a simply supported beam, a corbel, and a wall with a window are conducted. Clear steel trajectories of SRC structures can be obtained using both methods. The area of critical tensile stress in concrete yielded by the M-BESO is more than 40% lower than that yielded by the uniform design and BESO. Hence, the M-BESO facilitates a fully digital workflow that can be extremely effective for improving the design of steel reinforcements in concrete structures.

**KEYWORDS** bi-directional evolutionary structural optimization, steel-reinforced concrete, concrete stress, reinforcement method, hybrid model

## 1 Introduction

Concrete is the most widely used material in civil engineering and can balance performance, availability, and cost [1–3]. However, brittle stretching and quasi-brittle compression limit their application in complicated load cases. Steel-reinforced concrete (SRC) structures are widely used as alternatives to plain concrete [1–10]. The strength and ductility of concrete structures can be significantly improved by introducing steel reinforcements. An SRC structure may feature Bernoulli regions (B-regions) and disturbed regions (D-regions). B-regions can typically be designed well using the established beam theory and cross-sectional analysis, whereas the D-regions exhibit nonlinear deformation, to which conventional beam design methods are not applicable

[11]. Hence, the strut-and-tie model (STM) [12] has been used to analyze D-regions and design reinforcement layouts. The STM allows the behavior of an equivalent truss structure to be examined to investigate the performance of complex D-regions. In this truss analogy, the components under compression are known as struts, which are filled with concrete. Meanwhile, tie rods are used to brace tensile stress, and the connections between the struts and tie rods are known as nodes.

For an irregular SRC structure with complicated boundary conditions, obtaining an appropriate STM based on the designer's experience is challenging owing to the complex stress trajectories involved. Structural optimization techniques can be adopted to determine the optimized layout of steel reinforcements. STM optimization was first implemented using discrete topology optimization based on the truss ground structure approach [13,14]. In this method, the truss topology is described by

the truss members, whose cross-sectional areas are adopted as the design variables for optimization. Hence, the optimization of the STM is transformed into a generalized sizing problem. In the truss ground structure optimization, the cross-sectional areas of the ties change iteratively. The ties with cross-sectional areas smaller than the lower limit are removed from the final design. Based on the ground structure approach, Bontempi and Malerba [15] and Ali and White [16] proposed an automatic search technique to determine truss trajectories in a concrete matrix. In addition, genetic algorithms were used to determine the optimal layout of the locations of reinforcing ties and compressive struts in SRC beams [17]. However, topology optimization based on the truss ground structure defines the nodal locations and connections, thus limiting the STM configuration of an SRC structure.

The continuum topology optimization method [18,19] for optimizing SRC structures has garnered significant attention in recent years [20–26]. Several continuum topology optimization techniques have been developed in the past decades, e.g., the solid isotropic microstructures with penalization method [27], the bi-directional evolutionary structural optimization (BESO) method [28,29], the level set-based method [30–32], and the moving morphable component method [33]. These techniques have been used extensively in dynamic properties where uncertainty is considered [34], multidisciplinary research [35–40], and novel structure designs [41–44]. Liang et al. [20,21] applied the BESO technique to establish an STM for classical deep beams in civil engineering. Xia et al. [45] proposed a technique that comprises compliance-based topology optimization, topology extraction, and shape optimization to automatically generate a three-dimensional (3D) optimization-based STM. However, these studies only considered a single phase in topology optimization, which contradicts the fact that an SRC structure contains both concrete and steel. Hence, incorporating different mechanical properties of concrete and steel into the final structure is more reasonable [46–48].

In an STM, concrete struts represent compressive elements, whereas ties are under tension and form reinforcing bar (rebar) cages. However, rebar cages typically result in a high reinforcement ratio in an SRC structure, which is laborious to construct and difficult to infiltrate by concrete [49]. An alternative approach to enhance the performance of concrete is by using discrete steel bars or fibers [50,51]. Notably, steel bars under both tension and compression are acceptable in actual SRC structures. However, in the STM, steel bars are assumed to be only in tension. Furthermore, in STM-based optimizations, unnecessary concrete in compression is removed, and the tensile zone contains steel bars only, which affects the overall stiffness and actual internal

force distribution of the original structure. To benefit from both continuum and truss topology optimizations, Guest and Moen [52] combined the truss ground structure and continuum finite elements into a mesh of shared nodes, where tension members were presented by truss elements for steel reinforcement design, whereas continuum elements were used to discretize concrete. Subsequently, Gaynor et al. [53] investigated topology optimization based on a hybrid truss-continuum model, in which a bilinear truss-continuum topology optimization approach was used to prevent missing trusses in the solution for cases involving transverse tensile stresses caused by load spreading. More recently, Amir and Sigmund [54] presented a truss topology optimization method for embedding a truss ground structure into a concrete continuum. Yang et al. [55] investigated 3D force flow paths and reinforcement design in concrete via stress-dependent truss-continuum topology optimization. However, the stiffness of the truss steel element modeled using the hybrid approach was high in tension but negligible in compression. Material failure should be avoided in engineering practice. Meanwhile, Luo et al. [56] optimized an SRC structure under stiffness and strength constraints based on the Drucker–Prager criterion. Recently, Yang et al. [57] conducted a topology optimization of steel and concrete composites based on a truss-like material model and then solved it using the full stress method to design SRC structures. Pastore et al. [58] proposed an innovative optimization procedure based on an integrated risk factor and stress-constrained approach to design a lightweight SRC, in which the asymmetrical compression and traction strengths of concrete were considered comprehensively. Cui et al. [59] proposed a method to optimize the reinforcement layout of SRC structures under multiple load cases with stress constraints using a planar truss-like material model. Ghasemi et al. [60,61] optimized the distribution of short fibers in continuum concrete structures using an efficient gradient-based sequential optimization approach.

In summary, significant achievements have been achieved in the reinforcement design of SRC structures. However, the main disadvantages of the STM are its time-consuming implementation, absence of specialized computer software for practical design, and difficulty in redesigning the detailed reinforcement layout. Furthermore, the reinforcements obtained via optimization based on the classical truss-like ground structure formulation are non-continuous. Hence, the design of SRC structures should be fully digital in the future.

The aim of this study is to develop a BESO approach based on a truss-continuum hybrid model, which allows a fully digital workflow for the reinforcement design of complex SRC structures. In the new approach, reinforcing bars are modeled as truss elements embedded in continuum concrete. An optimized steel reinforcement

layout with both tension and compression elements in a constant concrete domain is obtained via BESO. Furthermore, a modified formulation using the stress state of the host concrete is constructed based on the BESO method. This method can optimize the layout of the truss while considering the stress distribution, thus eliminating the discreteness of conventional truss topology optimization based on the ground structure approach. The method proposed herein can automatically generate reinforcement for SRC structures, which facilitates the optimization of steel and concrete composites, thus mitigating concrete cracking and increasing structural stiffness. The findings of this study will allow civil engineers to conveniently improve the steel layout design of concrete structures.

## 2 Finite element model

### 2.1 Finite element model of steel truss

In topology optimization, structural analysis is performed using the finite element method. Concrete and reinforcing steel in SRC were simulated using different material models, and a perfect bond between the two materials was assumed. Each steel reinforcing bar was modeled using a truss element embedded in a two-dimensional (2D) concrete element. The same method was previously adopted by Kwak and Filippou [62].

As the purpose of this study is to verify the proposed heuristic orientation-identification system instead of generating a complicated reinforcement layout, only four types of embedded trusses were considered to simplify the problem, where reinforcing bars were placed horizontally, vertically, or in two diagonal forms [55]. The truss orientations were defined in four groups, i.e., 0°, 45°, 90°, and 135° in the anticlockwise direction from the  $x$ -axis, as shown in Fig. 1.

Figure 1 shows the truss model for the steel reinforcement. In the global coordinate system, the displacements of the two nodes, e.g., A and B, in element- $i$  form a displacement vector, i.e.,

$$\mathbf{u}_i = [u_A \ v_A \ u_B \ v_B]^T. \quad (1)$$

The strain energy of the truss element is written as

$$U_i = \frac{1}{2} \mathbf{u}_i^T \mathbf{L}_i^T \mathbf{k}'_i \mathbf{L}_i \mathbf{u}_i, \quad (2)$$

where  $\mathbf{L}_i$  is the transformation matrix, expressed as

$$\mathbf{L}_i = \begin{bmatrix} \cos\theta & \sin\theta & 0 & 0 \\ 0 & 0 & \cos\theta & \sin\theta \end{bmatrix}, \quad (3)$$

where  $\mathbf{k}'_i$  is the elemental stiffness matrix in the local coordinate system of the truss, i.e.,  $(EA_i/L_i)\mathbf{I}$ , where  $E$  is the Young's modulus of steel,  $A_i$  is the truss area,  $L_i$  is the truss length, and  $\mathbf{I}$  is a  $2 \times 2$  unit matrix. In the global coordinate system, the elemental stiffness matrix  $\mathbf{k}_i$  of the truss element can be expressed as follows:

$$\mathbf{k}_i = \mathbf{L}_i^T \mathbf{k}'_i \mathbf{L}_i = \frac{EA_i}{L_i} \cdot \begin{bmatrix} \cos^2\theta & \cos\theta\sin\theta & -\cos^2\theta & -\cos\theta\sin\theta \\ \cos\theta\sin\theta & \sin^2\theta & -\cos\theta\sin\theta & -\sin^2\theta \\ -\cos^2\theta & -\cos\theta\sin\theta & \cos^2\theta & \cos\theta\sin\theta \\ -\cos\theta\sin\theta & -\sin^2\theta & \cos\theta\sin\theta & \sin^2\theta \end{bmatrix}. \quad (4)$$

In this study,  $\mathbf{k}_i$  was subjected to four reinforcing-bar orientations, as shown in Fig. 1.

### 2.2 Hybrid truss-continuum computing formulation

As shown in Fig. 1(c), a hybrid truss-continuum structure comprises a steel truss embedded in a concrete matrix. The two components of the hybrid structure share the same nodes. In this study, concrete is regarded as a non-design material, i.e., its distribution remains unchanged during the optimization process. To achieve an almost solid-void design, the Young's modulus of the intermediate material was interpolated as a function of the density of the steel truss element as follows:

$$E_s(x_{s,i}) = E_s^0 x_{s,i}^p, \quad E_c = E_c^0, \quad (5)$$

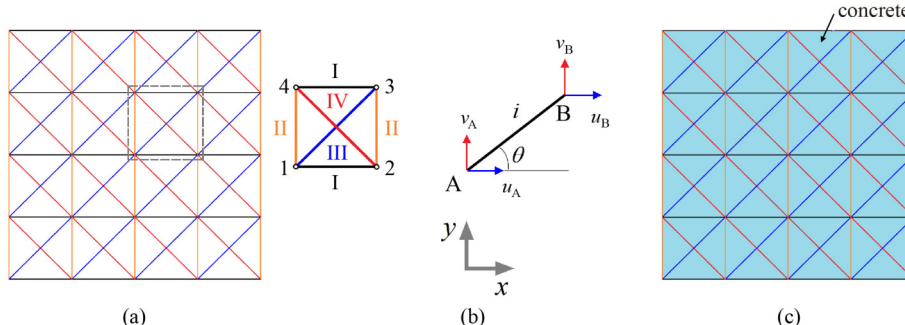


**Fig. 1** 2D truss element model for steel reinforcement in concrete: (a) orthogonal-diagonal steel bar model with four types of truss elements; (b) truss element- $i$  with orientation  $\theta$ ; (c) steel-reinforced concrete structure with steel trusses embedded in concrete matrix.

where  $E_s^0$  denotes the Young's modulus of the solid material,  $x_{s,i}$  denotes the density of the truss element,  $p$  denotes the penalty exponent for the truss element, and  $E_c^0$  denotes the Young's modulus of concrete. To clarify the two materials, subscripts "s" and "c" are used herein to represent steel and concrete, respectively.

The classical four-node plane-stress quadrilateral element was used to discretize the concrete structure. The element stiffness of concrete  $\mathbf{k}_c$  is expressed as

$$\mathbf{k}_c = t \mathbf{A} \mathbf{B}^T \mathbf{D} \mathbf{B}, \quad (6)$$

where  $t$  is the thickness of concrete,  $A$  is the area of the element,  $\mathbf{D}$  is the elasticity matrix of concrete, and  $\mathbf{B}$  is the displacement-strain vector of the four-node plane-stress quadrilateral element. Subsequently, the global stiffness matrix of concrete  $\mathbf{K}_c$  can be expressed as

$$\mathbf{K}_c = \langle \mathbf{k}_{c,i} \rangle_{i=1}^{n_c}, \quad (7)$$

where  $\langle \rangle$  denotes the assembling operator of the stiffness matrix.

In this study, the Poisson's ratio is assumed to be independent of the design variables ( $x_{s,i}$ ). The elemental stiffness matrix is a function of the design variables, and the global matrix of the steel truss is expressed as

$$\mathbf{K}_s = \langle \mathbf{k}_{s,i} \rangle_{i=1}^{n_s} = \langle x_{s,i}^p \mathbf{k}_{s,i}^0 \rangle_{i=1}^{n_s}, \quad (8)$$

where  $\mathbf{k}_{s,i}^0$  denotes the element stiffness matrix of truss- $i$  when  $x_{s,i} = 1$ .

Furthermore, the assembled global stiffness matrix  $\mathbf{K}$  can be obtained by adding the global stiffness matrix of steel  $\mathbf{K}_s$  to the global stiffness matrix of concrete  $\mathbf{K}_c$  based on the superposition principle. Hence, the equilibrium equation of the hybrid structure can be expressed as

$$\mathbf{KU} = (\mathbf{K}_s + \mathbf{K}_c) \mathbf{U} = \mathbf{F}. \quad (9)$$

In the computing scheme of the hybrid truss-continuum model, the stress of the concrete element can be calculated as follows:

$$\boldsymbol{\sigma}_c = \mathbf{D}_0 \boldsymbol{\varepsilon}_c = \mathbf{D}_0 \mathbf{B} \mathbf{u}, \quad (10)$$

where  $\boldsymbol{\sigma}_c$  and  $\boldsymbol{\varepsilon}_c$  represent the stress and strain of the concrete element,  $\mathbf{D}_0$  denotes the element stiffness matrix, and  $\mathbf{u}$  is the displacement vector.

### 3 Topology optimization algorithm

Based on the hybrid truss-continuum computing formulation, BESO can be extended to optimize the reinforcement layout in an SRC structure. Herein, a new method is proposed by modifying the BESO method, i.e., by considering a tensile stress constraint.

#### 3.1 Basic optimization formulation

In this section, the optimal design of a structure with maximum stiffness and minimum compliance is discussed. During the optimization, the concrete matrix remained unchanged, and the steel trusses changed gradually. Mathematically, the optimization model for an SRC structure can be expressed as

$$\begin{cases} \text{Min } C = \frac{1}{2} \mathbf{U}^T \mathbf{K} \mathbf{U}, \\ \text{s.t. } (\mathbf{K}_s + \mathbf{K}_c) \mathbf{U} = \mathbf{F}, \\ V(\mathbf{x}_s) = \sum x_{s,i} v_i - V_{fs} = 0, \\ x_{s,i} \in \{\rho_{\min}, 1\}, \quad (i = 1, 2, \dots, N_s) \end{cases} \quad (11)$$

where  $C$  represents structural compliance;  $\mathbf{K}$ ,  $\mathbf{U}$ , and  $\mathbf{F}$  are the global stiffness matrix, global displacement, and load vector, respectively;  $v_i$  is the volume of the truss- $i$  element;  $V(\mathbf{x}_s)$  is the total volume of the truss elements in the  $i$ -th iteration; and  $V_{fs}$  is the prescribed target volume fraction of the steel component. The lower bound  $\rho_{\min}$  was set to 0.001 in this study.

The sensitivity of the objective function is written as

$$\frac{\partial C}{\partial x_{c,i}} = \frac{1}{2} \frac{\partial \mathbf{F}^T}{\partial x_{c,i}} \mathbf{U} + \frac{1}{2} \mathbf{F}^T \frac{\partial \mathbf{U}}{\partial x_{c,i}}. \quad (12)$$

The adjoint method was used to determine the sensitivity of the displacement vector by introducing a vector of the Lagrangian multiplier  $\lambda$ . Because of the equilibrium, as expressed in Eq. (9), the objective function in Eq. (11) can be modified by adding an additional term  $\lambda^T (\mathbf{F} - \mathbf{K} \mathbf{U})$  as follows [63]:

$$C = \frac{1}{2} \mathbf{F}^T \mathbf{U} + \lambda^T [\mathbf{F} - (\mathbf{K}_s + \mathbf{K}_c) \mathbf{U}]. \quad (13)$$

The sensitivity of the modified objective function can be written as

$$\begin{aligned} \frac{\partial C}{\partial x_{s,i}} &= \frac{1}{2} \frac{\partial \mathbf{F}^T}{\partial x_{s,i}} \mathbf{U} + \frac{1}{2} \mathbf{F}^T \frac{\partial \mathbf{U}}{\partial x_{s,i}} + \frac{\partial \lambda^T}{\partial x_{s,i}} [\mathbf{F} - (\mathbf{K}_s + \mathbf{K}_c) \mathbf{U}] \\ &\quad + \lambda^T \left[ \frac{\partial \mathbf{F}}{\partial x_{s,i}} - \frac{\partial \mathbf{K}_s}{\partial x_{s,i}} \mathbf{U} - (\mathbf{K}_s + \mathbf{K}_c) \frac{\partial \mathbf{U}}{\partial x_{s,i}} \right]. \end{aligned} \quad (14)$$

The third term in Eq. (14) becomes zero because of the equilibrium of the structure. In addition, the applied load is assumed to be unaffected by the variation in an element; therefore,  $\frac{\partial \mathbf{F}}{\partial x_{s,i}} = 0$ . Thus, the sensitivity is written as

$$\frac{\partial C}{\partial x_{s,i}} = \left[ \frac{1}{2} \mathbf{F}^T - \lambda^T (\mathbf{K}_s + \mathbf{K}_c) \right] \frac{\partial \mathbf{U}}{\partial x_{s,i}} - \lambda^T \frac{\partial \mathbf{K}_s}{\partial x_{s,i}} \mathbf{U}. \quad (15)$$

Because  $(\mathbf{F} - \mathbf{K} \mathbf{U})$  is equal to zero, the Lagrangian multiplier vector  $\lambda$  can be selected arbitrarily. To

eliminate the unknown  $\frac{\partial \mathbf{U}}{\partial x_{s,i}}$  in Eq. (15), the value of  $\lambda$  [63] shall satisfy

$$\frac{1}{2} \mathbf{F}^T - \lambda^T (\mathbf{K}_s + \mathbf{K}_c) = 0. \quad (16)$$

Based on a comparison between Eqs. (16) and (9), the solution for the Lagrangian multiplier vector  $\lambda$  [63] is as follows:

$$\lambda = \frac{1}{2} \mathbf{U}. \quad (17)$$

By substituting  $\lambda$  into Eq. (15), the sensitivity is expressed as

$$\frac{\partial C}{\partial x_{s,i}} = -\frac{1}{2} \mathbf{U}^T \frac{\partial \mathbf{K}_s}{\partial x_{s,i}} \mathbf{U}. \quad (18)$$

When the material interpolation scheme expressed in Eq. (8) is used, the sensitivity can be written as

$$\frac{\partial C}{\partial x_{s,i}} = -\frac{1}{2} p x_{s,i}^{p-1} \mathbf{u}_i^T \mathbf{k}_{s,i}^0 \mathbf{u}_i, \quad (19)$$

where  $\mathbf{u}_i$  is the nodal displacement vector of element- $i$ .

In the BESO, a structure is optimized using discrete design variables, i.e., the design variables are either lower boundaries or 1. Therefore, the sensitivity number of the basic formulation can be defined by the relative ranking of the sensitivities of the elements, as follows:

$$\alpha_i = -\frac{1}{p} \frac{\partial C}{\partial x_{s,i}} = \begin{cases} \frac{1}{2} \mathbf{u}_i^T \mathbf{k}_{s,i}^0 \mathbf{u}_i, & \text{when } x_{s,i} = 1, \\ \frac{x_{\min}^{p-1}}{2} \mathbf{u}_i^T \mathbf{k}_{s,i}^0 \mathbf{u}_i, & \text{when } x_{s,i} = x_{\min}. \end{cases} \quad (20)$$

The raw sensitivity above should be smoothed using a filtering method to achieve a mesh-independent solution before updating the design variable [64–66]. The details are as follows:

$$\hat{\alpha}_i = \frac{\sum_{j=1}^{nel} \omega_{ij} \alpha_j}{\sum_{j=1}^{nel} \omega_{ij}}, \quad (21a)$$

$$\omega_{ij} = \max(0, r_{\min} - r_{ij}), \quad (21b)$$

where  $nel$  is the number of neighboring elements,  $r_{ij}$  is the distance between the centroids of central element- $i$  and its neighboring element- $j$ ,  $\omega_{ij}$  is the weight function ( $0 \leq \omega_{ij} < 1$ ), and  $r_{\min}$  is the filter radius.

Based on the steel bar orientations shown in Fig. 1, the sensitivity numbers were classified into four groups. To obtain a more reasonable reinforcement layout, the

sensitivity was filtered separately for the four types of trusses using the mid-point of each bar as the center of the filtering circle (red dots in Fig. 2). Using type I and type III as examples, the filter regions for each truss sensitivity group are shown in Fig. 2, where the marked red lines represent the trusses involved in the filtering calculation.

The BESO technique for these formulations is as follows: To achieve a more stable iterative procedure, the sensitivity number for the current iteration  $k$  is regarded as the average of the sensitivity numbers in the current and previous two iterations, which is expressed as

$$\hat{\alpha}_i^{(k)} = \frac{1}{3} (\hat{\alpha}_i^{(k)} + \hat{\alpha}_i^{(k-1)} + \hat{\alpha}_i^{(k-2)}). \quad (22)$$

Before the elements are removed from or added to the current design iteration, the target volume for the next iteration  $V^{(k+1)}$  must be determined. The evolution of the material volume in each iteration is defined as

$$V^{(k+1)} = V^{(k)}(1 - ER), \quad (23)$$

where  $ER$  is the evolutionary volume ratio. The volume of the material remains constant for the remaining iterations once it reaches the objective volume, i.e.,

$$V^{(k+1)} = V_{fs}. \quad (24)$$

In the BESO, the sensitivity numbers of all truss elements, both solid and void, are organized based their sensitivity numbers (from the highest to the lowest). Because the modified sensitivity numbers include positive, zero, and negative values, void elements may be placed in the middle position during the sorting process. Hence, two evolutionary ratios were used to add or delete solid and void elements separately. To stably control the elemental deletion/addition, the evolutionary volume ratios of deletion  $ER_{\text{del}}$  and addition  $ER_{\text{add}}$  were defined as follows:

$$ER = ER_{\text{del}} - ER_{\text{add}}. \quad (25)$$

When the volume fraction satisfies Eq. (24),  $ER_{\text{add}} = ER_{\text{del}}$ . Therefore, the number of elements to be added is

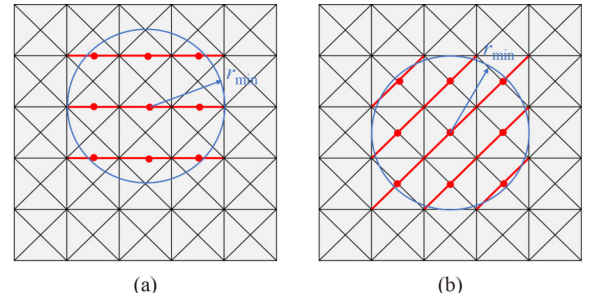


**Fig. 2** Filter regions of two types of truss members: (a) type I and (b) type III.

$$N_{\text{del}} = N \times V^{(k)} \times ER_{\text{del}}. \quad (26)$$

Meanwhile, the number of elements to be deleted is

$$N_{\text{add}} = N \times V^{(k)} \times ER_{\text{add}}. \quad (27)$$

Solid element (1) is removed (switched to 0) if

$$\hat{\alpha}_i \leq \alpha_{\text{del}}^{\text{th}}. \quad (28)$$

Void elements (0) are added (switched to 1) if

$$\hat{\alpha}_i > \alpha_{\text{add}}^{\text{th}}, \quad (29)$$

where  $\alpha_{\text{del}}^{\text{th}}$  and  $\alpha_{\text{add}}^{\text{th}}$  are the threshold sensitivity numbers for removing and adding elements, respectively; and  $\alpha_{\text{del}}^{\text{th}}$  is always less than or equal to  $\alpha_{\text{add}}^{\text{th}}$ . The number of added and deleted elements can be calculated using the dichotomy algorithm as follows [63]. First,  $\alpha_{\text{add}}^{\text{th}}$  is calculated by sorting the sensitivity number of void elements (0). The number of elements to be switched from zero to one is equal to  $N_{\text{add}}$  in the design domain.  $\alpha_{\text{add}}^{\text{th}}$  is the sensitivity number of the elements ranked immediately below the last added element. Subsequently, the sensitivity number of solid elements (1) is sorted, and  $\alpha_{\text{del}}^{\text{th}}$  is determined such that the number of removed elements is equal to  $N_{\text{del}}$ .

The optimization is terminated when the stress constraint, volume constraint, and convergence criterion are satisfied. The convergence criterion is defined in terms of the change in the objective value and is expressed as

$$\frac{\left| \sum_{i=1}^M C^{(k-i+1)} - \sum_{i=1}^M C^{(k-M-i+1)} \right|}{\sum_{i=1}^M C^{(k-i+1)}} \leq \tau, \quad (30)$$

where  $k$  is the current iteration number,  $\tau$  is the allowable convergence tolerance, and  $M$  is an integer. For example,  $M = 5$  implies that the change in the mean compliance over the last 10 iterations is sufficiently small, e.g.,  $\tau = 10^{-5}$  [63].

### 3.2 Stress-based sensitivity modification

The optimized topology was achieved using the relative ranking of the sensitivity numbers via the BESO. Regardless of whether an individual truss element is in tension or compression along its longitudinal axial direction, its corresponding sensitivity participates in the optimization algorithm. However, the resulting topology based on the contribution of steel reinforcement to the objective function may not reflect the actual design problem. Some steel reinforcements may remain in the compression regions owing to their sensitivities, which

are higher than those in the tension areas. To embed the maximum number of steel bars in areas of high tensile stress, a modified scheme is proposed and incorporated into the BESO algorithm to update the design variables by considering the stress state of the host concrete. The details of the proposed scheme are as follows.

In the truss-continuum combined model, the stress state  $\boldsymbol{\sigma}_i = [\sigma_{xx}, \sigma_{yy}, \tau_{xy}]$  at the center of the concrete shell element- $i$  (red dots in Fig. 3) can be obtained using Eq. (10). To smooth the stress field of the concrete, the filter method is used to obtain the stress state of each node (red stars in Fig. 3) as follows:

$$\hat{\boldsymbol{\sigma}}_i = \frac{\sum_{j=1}^n \omega_{ij}^{(s)} \boldsymbol{\sigma}_i}{\sum_{j=1}^n \omega_{ij}^{(s)}}, \quad (31a)$$

$$\omega_{ij}^{(s)} = \max(0, r_{ij}^{(s)} - r_{\min}^{(s)}), \quad (31b)$$

where  $n$  is the number of neighboring elements;  $r_{ij}^{(s)}$  denotes the distance between node- $i$  and its neighboring concrete element- $j$ ;  $\omega_{ij}^{(s)}$  denotes the weight function; and  $r_{\min}^{(s)}$  denotes the filter radius of the stress, as shown in Fig. 3.

Subsequently, the  $\sigma_{xx}$ ,  $\sigma_{yy}$ , and  $\tau_{xy}$  for each node in the concrete shell element can be obtained. The stress state of the host concrete at the center of each truss can be calculated by averaging the nodal stresses of the truss element as follows:

$$\boldsymbol{\sigma} = \frac{1}{2} (\boldsymbol{\sigma}_{N1} + \boldsymbol{\sigma}_{N2}), \quad (32)$$

where  $\boldsymbol{\sigma}_{N1}$  and  $\boldsymbol{\sigma}_{N2}$  are the stress states of the first and second nodes in a truss element, respectively, as shown in Fig. 3.

To consider the stress state of the host concrete in topology optimization, the basic sensitivity can be

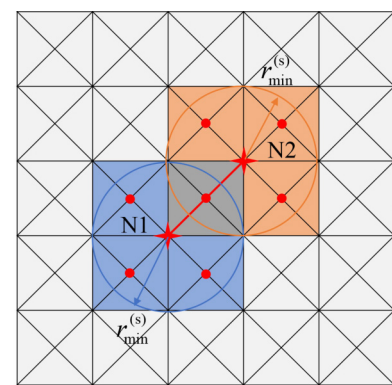


**Fig. 3** Stress state calculation of host concrete around truss element.

modified by multiplying the stress value of the host concrete as follows:

$$\hat{\alpha}_i = \hat{\alpha}_i^0 \sigma_{i,n}, \quad (33)$$

where  $\hat{\alpha}_i^0$  is the filtered sensitivity of the basic topology optimization formulation. The normal stress at any angle can be calculated as follows:

$$\sigma_n = \frac{1}{2}(\sigma_x + \sigma_y) + \frac{1}{2}(\sigma_x - \sigma_y)\cos 2\theta + \tau_{xy}\sin 2\theta. \quad (34)$$

Considering the steel bar orientations shown in Fig. 1, directional angles of  $0^\circ$ ,  $45^\circ$ ,  $90^\circ$ , and  $135^\circ$  were adopted for truss bars I, II, III, and IV, respectively, to calculate the stress in the host concrete.

Herein, a stress-based modified formulation (Eq. (22)) based on the basic BESO method, known as the modified BESO (M-BESO), is proposed. To evaluate the entire stress state of the host concrete, an evaluation ratio is proposed herein, which is based on the volume fraction of elements whose first principal stresses (FPSs) exceed the critical tensile stress.

$$R_{\text{FPS} > \sigma_t} = \frac{N_{\text{FPS} > \sigma_t}}{N_c} \times 100\%, \quad (35)$$

where  $N_{\text{FPS} > \sigma_t}$  is the number of concrete elements whose FPS exceeds the tensile strength,  $N_c$  is the total number of concrete elements, and  $R_{\text{FPS} > \sigma_t}$  is the volume fraction of concrete in a critical stress state. The FPS can be calculated as follows:

$$\sigma_{\text{FPS}} = \frac{1}{2}(\sigma_x + \sigma_y) + \sqrt{\left(\frac{\sigma_x - \sigma_y}{2}\right)^2 + \tau_{xy}^2}. \quad (36)$$

In this study, a critical tensile stress of 2 MPa was used for concrete [67]; thus,  $R_{\text{FPS} > 2}$  was accepted as the evaluation criterion.

### 3.3 Procedures of 2D truss-continuum topology optimization

The procedures of the proposed 2D truss-continuum topology optimization include the following 13 primary steps.

Step 1 Discretize the initial design domain with specific boundary conditions, and initialize the design variables  $\mathbf{x}_s$ .

Step 2 Assign optimization parameters to the algorithm.

Step 3 Conduct finite element analysis.

Step 4 Calculate the sensitivities of the truss elements in the design domain.

Step 5 Filter the sensitivities of types I, II, III, and IV trusses separately.

Step 6 Calculate the stress of each concrete element.

Step 7 Filter the stress states and obtain the stress of

concrete on each node.

Step 8 Determine the stress of the host concrete around the truss element along four orientations.

Step 9 Modify the sensitivities of the truss elements based on the stress state.

Step 10 Obtain the average of the sensitivities using the history information.

Step 11 Update the design variables by adding and deleting elements.

Step 12 Return to Step 3 if the volume constraint or convergence criterion is not satisfied.

Step 13 Stop for post-processing.

The flowchart of the proposed method is presented in Fig. 4.

---

## 4 Numerical examples

This section presents four examples to demonstrate the performance of the proposed approach. Four-node quadrilateral plane-stress elements were used to discretize the 2D concrete structure. The steel trusses share the same nodes at the joints, as shown in Fig. 1(c). In all cases, both the concrete and steel materials were assumed to be linearly elastic. The thickness of the concrete component was 30 mm, and the cross-sectional area of the steel reinforcing bar was  $78.5 \text{ mm}^2$  (diameter, 10 mm). The Young's moduli of steel and concrete ( $E_c$ ) were 210 and 5 GPa, respectively. The Poisson's ratio of both the steel and concrete was 0.3. The values for the basic parameters used in the BESO and M-BESO were fixed; for example, the filter radius for the design variables  $r_{\min}$  is 3.0 times the element size, and the evolutional ratios are  $ER_{\text{del}} = 2\%$  and  $ER_{\text{add}} = 0.5\%$ . The filter radius for stress  $r_{\min}^{(s)}$  in the M-BESO method is 1.5.

### 4.1 Simply supported beam

Figure 5(a) shows a simply supported beam under an in-plane vertical load ( $F$ ) of 100 kN at the bottom center. This example is presented to demonstrate the accuracy and convergence of the proposed hybrid truss-continuum structure. The beam measured  $10 \text{ m} \times 2.5 \text{ m}$ . The left and right ends of the beam were constrained. The target volume fraction of the truss elements was  $V_{fs} = 20\%$ , which yields a reinforcement ratio of 1.28% from the initial over-reinforcement (6.4%). In this study, the unit mesh size was selected based on the sizes of the steel bar and overall structure. The design domain contained 2500 unit hybrid truss-continuum elements with a unit mesh measuring  $0.1 \text{ m} \times 0.1 \text{ m}$ . To optimize the layout of the steel trusses for reinforcing the concrete structure, BESO was employed. To reduce the overall tensile stress level of the host concrete, the M-BESO algorithm was applied to the simply supported beam.

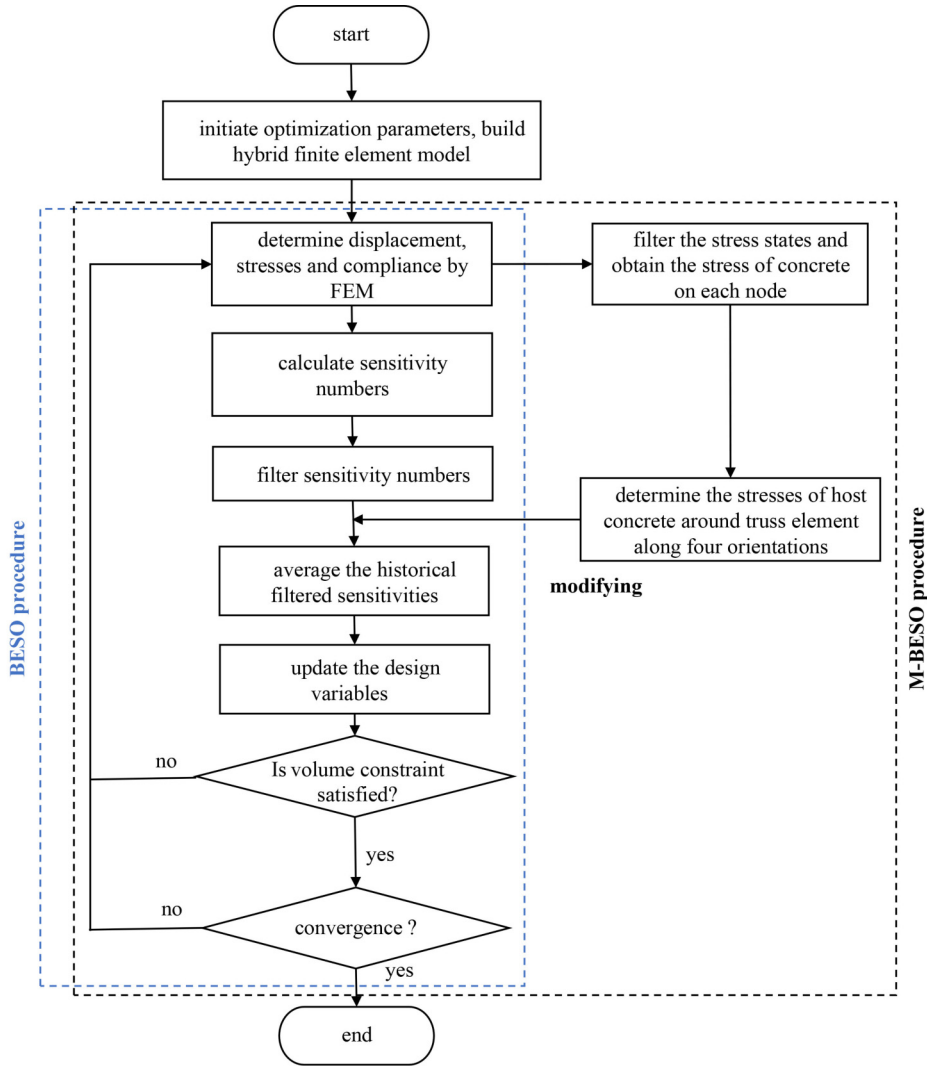


**Fig. 4** Flowchart of BESO and M-BESO methods.

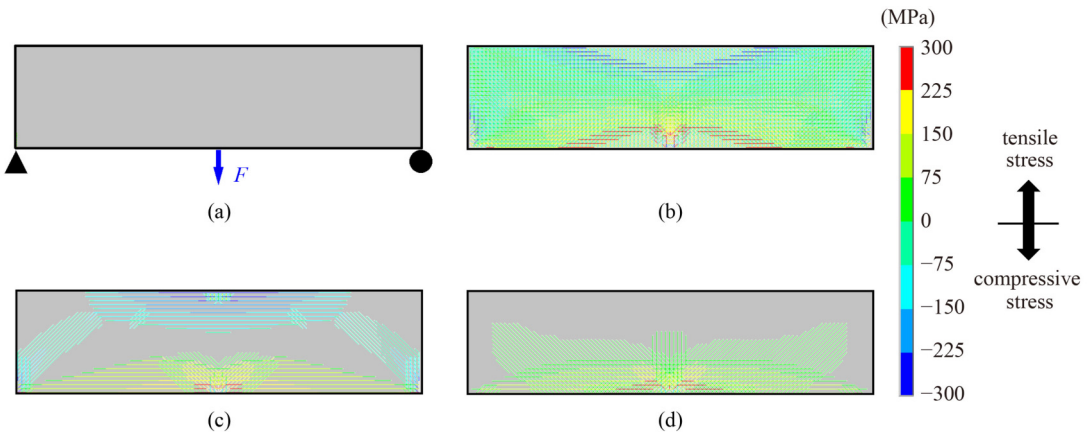


**Fig. 5** Simply supported beam: (a) structure; (b) uniform trusses; (c) optimized steel truss layout obtained via BESO; (d) optimized steel truss layout obtained via M-BESO. (In the color bar, the positive and negative values denote tensile and compressive stresses, respectively.)

To evaluate the effectiveness of the two methods in optimizing the layout of steel reinforcement in concrete structures, finite element analysis was conducted based

on the two optimized results, as well as for reinforced concrete comprising uniform steel bars with a cross-sectional area of  $15.7 \text{ mm}^2$ , which features the same steel

reinforcement ratio as the optimized results. Based on Fig. 5(b), most of the rebars in the upper section of the uniform layout were under compression, whereas the lower section was under tension. The final layouts of the steel trusses obtained via both the BESO and M-BESO methods show clear but different rebar trajectories, as shown in Figs. 5(c) and 5(d). For example, the trusses in the BESO solution formed a closed loop. However, the upper section and the loop arches were under compression. In the topology yielded by the M-BESO, the upper trusses disappeared, and the diagonal reinforcing bars at the bottom position were extended. All trusses in the M-BESO solution showed tensile axial stresses, as shown in Fig. 5(d), which indicates that all trusses in the M-BESO solution can be utilized to withstand tension. Hence, the stress-based modified sensitivity affected the topology of the steel truss layout.

The features of the truss layout obtained from the BESO solution (Fig. 5(c)) were similar to those of the linear elastic rebar-based topology optimization proposed by Amir and Sigmund (Fig. 6(a)) [54]. Damage-based optimization was further performed by Amir and Sigmund (Fig. 6(b)) [54], which resulted in efficient structures with a higher load-bearing capacity per unit weight compared with linear elastic rebar-based topology optimization. The reinforcement pattern yielded by the M-BESO solution (Fig. 5(d)) was similar to that yielded by the damage-based optimization (Fig. 6(b)). Therefore, the M-BESO method can be regarded as a comparable strength-based optimization method for reinforcement in SRC structures. The layout mode of the M-BESO solution was validated by Yang et al. [57] and Cui et al. [59] using a composite truss-like model, as shown in Figs. 6(c) and 6(d), respectively. Unlike their discrete reinforcements, the proposed M-BESO provides a more continuous reinforcement distribution, which is beneficial

for engineering applications.

After 125 iterations, the BESO and M-BESO solutions converged, as shown in Fig. 7. The compliance and  $R_{FPS > 2}$  of both methods remained stable when approaching convergence. The  $R_{FPS > 2}$  of the M-BESO solution varied slightly during the iteration, whereas that of the BESO solution increased rapidly. This implies that the M-BESO allows the FPS field to be controlled during optimization.

The compliance and critical tensile stress area ratios  $R_{FPS > 2}$  of the three structures are listed in Table 1. Compared with the results of the uniform structure, the compliance of the BESO solution decreased by 37.7% but its  $R_{FPS > 2}$  increased by 7.5%. Compared with the  $R_{FPS > 2}$  of the uniform structure and BESO solution, the  $R_{FPS > 2}$  of the M-BESO solution decreased by 48.8% and 52.4%, respectively. Moreover, the compliance of the M-BESO solution was 2145.9 N·m, which was slightly lower (by 8%) than that of the structure with uniform steel trusses. The high FPS field of concrete was reduced by the M-BESO method, which slightly reduced the stiffness of the SRC structure.

The FPS contours of the three structures are shown in Fig. 8. The critical tensile stress area of the concrete ( $FPS > 2$  MPa) in the M-BESO solution was the smallest among the three structures. In the uniform structure, stress concentrations were indicated around the loading and constraint points, and the critical tensile stress was indicated in the lower section of the concrete. The BESO solution can significantly reduce the stress concentrations but not the critical tensile stresses. As all the rebars were arranged at the lower section, the critical tensile stress area can be reduced significantly. The stress contours of concrete indicate the effectiveness of the present M-BESO in arranging steel reinforcements in SRC structures for controlling the tensile stress level of the host concrete.

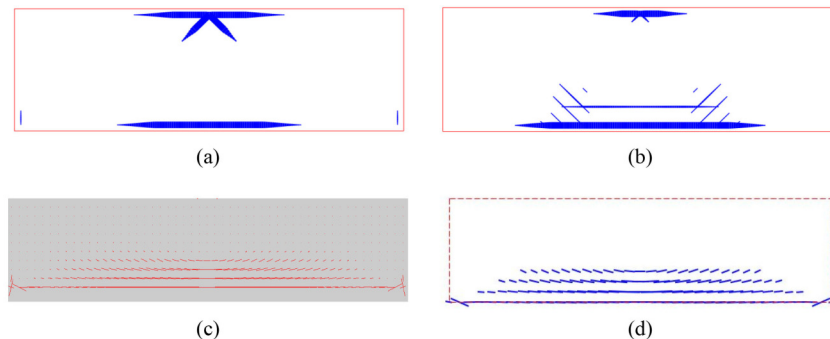


**Fig. 6** Reinforcements of simply supported beam: (a) linear elastic rebars and (b) damage-based embedded rebars from Amir and Sigmund [54] (Reprinted from Structural and Multidisciplinary Optimization, 47(2), Amir O, Sigmund O, Reinforcement layout design for concrete structures based on continuum damage and truss topology optimization, 157–174, Copyright 2013, with permission from Springer.), (c) Yang et al. [57] (Reprinted from Structural and Multidisciplinary Optimization, 67(1), Yang Z, Zhou K, Qiao S, Topology optimization of reinforced concrete structure using composite truss-like model, 79–85, Copyright 2018, with permission from Techno.), and (d) Cui et al. [59] (Reprinted from Latin American Journal of Solids and Structures, 17(4), Cui H, Zhou K, Yang Z, Reinforcement layout design of RC structures under multiple load cases using truss-like material model, 17, Copyright 2020, with permission from MARCÍLIO ALVES LAJSS.).

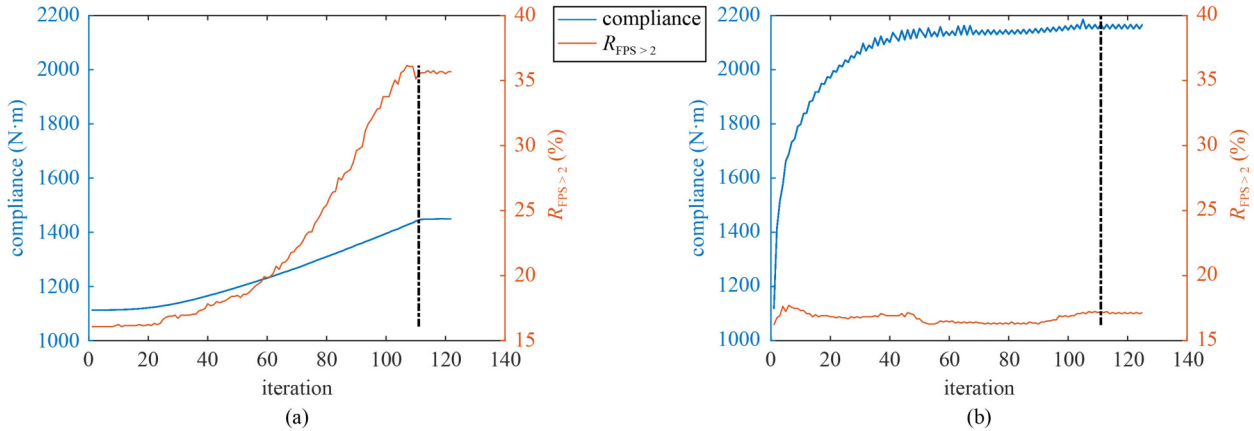


**Fig. 7** Evolutions of the objective function ( $C(0) = 1112.4 \text{ N}\cdot\text{m}$ ) and risk ratio ( $R_{\text{FPS} > 2}(0) = 16.1\%$ ) for simply supported beam: (a) BESO and (b) M-BESO results. Dashed line represents the volume fraction constraint.

**Table 1** Compliance and  $R_{\text{FPS} > 2}$  for simply supported beams with different truss layouts

indicator	$C (\text{N}\cdot\text{m})$	$R_{\text{FPS} > 2} (\%)$
uniform	2325.4	33.2
BESO	1449.7	35.7
M-BESO	2145.9	17.0

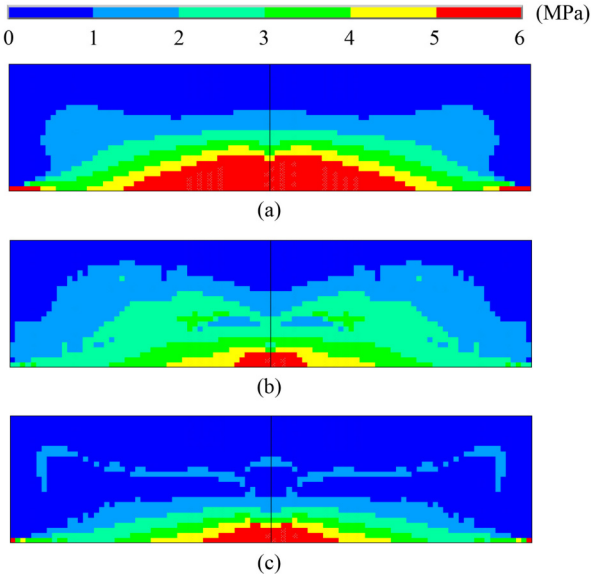


**Fig. 8** FPS contours of simply supported beam: (a) structure with uniform steel reinforcement; (b) BESO results; (c) M-BESO results.

#### 4.2 Corbel

Reinforced-concrete corbels are typical D-regions used in building structures to support precast beams. The 2D corbel shown in Fig. 9(a) was under an in-plane vertical load ( $F$ ) of 500 kN. The upper and lower ends of the structure were fixed. The target volume fraction of the truss elements was  $V_{\text{fs}} = 20\%$ , i.e., the reinforcement ratio

was reduced to 1.23% from the initial value of 6.15%. The design domain contained 2832 unit hybrid truss-continuum elements, and the unit mesh measured  $0.025 \text{ m} \times 0.025 \text{ m}$ . The proposed BESO and M-BESO methods were employed for the steel reinforcement design of the corbel.

Finite element analysis was performed on the SRC corbel comprising uniformly distributed steel reinforcing bars with a cross-sectional area of  $15.7 \text{ mm}^2$ , which resulted in the same volume of steel reinforcement as the optimization results. As illustrated in Fig. 9(b), most of the rebars in the upper section was under tension, whereas most of the rebars in the lower section were under compression. After 115 iterations, the final layouts of the steel trusses determined via the BESO and M-BESO were plotted, as shown in Figs. 9(c) and 9(d), respectively. In addition to the rebars in the loading area, the truss layout in the BESO solution was an approximately symmetric structure connecting the left corners of the two fixed ends and the point under load. However, the lower trusses of the layout were compressed. In the layout obtained via the M-BESO, most of the rebars were arranged in the upper section. In the high tensile stress areas, the trusses improved as compared with the BESO solution. Moreover, the trusses at the lower section of the M-BESO solution were stretched.

In the STM-based corbel design of Liang et al. (Fig. 10(a)) [20], the applied load was transferred to the entire structure along the paths of the compressive struts and tensile ties. Unlike the STM, the truss layout of the M-BESO solution illustrated in Fig. 9(d) is similar to the path of the tensile ties. The layout trajectories of the M-BESO solution were consistent with the result of Cui et al. (Fig. 10(b)) [59], which was based on a truss-like material model. However, Cui et al. [59] used discrete members in their design, whereas a continuous reinforcement layout was generated by the M-BESO solution. The damaged areas in the corbel analyzed by Amir [68] are illustrated in Figs. 10(c) and 10(d). Most of the

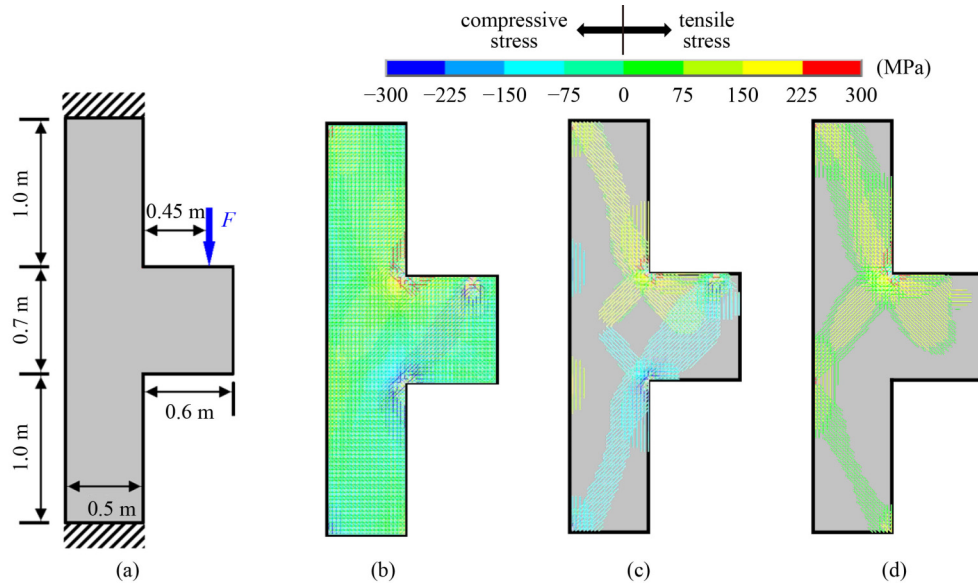


**Fig. 9** Corbel numerical examples: (a) structure; (b) uniform trusses; (c) optimized steel truss layout obtained via BESO; (d) optimized steel truss layout obtained via M-BESO method.

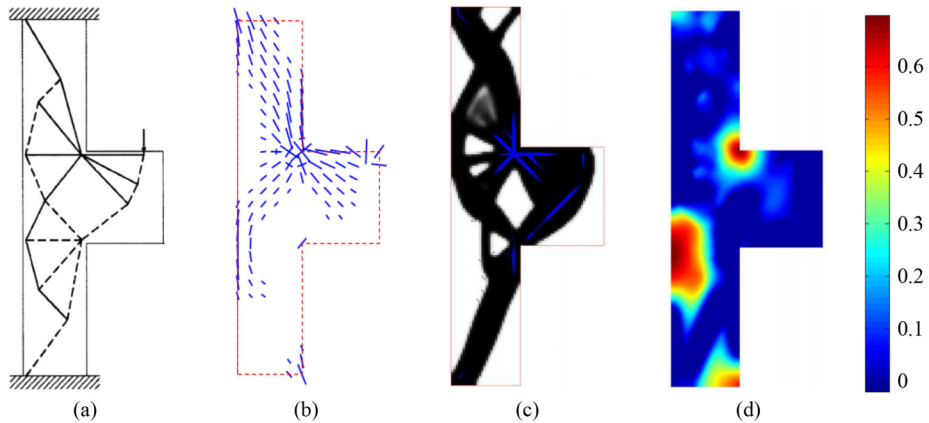


**Fig. 10** Corbel examples: (a) STM from topology optimization by Liang et al. [20] (Authorized reprint from ACI Materials Journal, 97(2), 2000, Liang Q Q, Xie Y M, Steven G P, Topology optimization of strut and-tie models in reinforced concrete structures using an evolutionary procedure.); (b) reinforcement layout by Cui et al. [59] (Reprinted from Latin American Journal of Solids and Structures, 17(4), Cui H, Zhou K, Yang Z, Reinforcement layout design of RC structures under multiple load cases using truss-like material model, 17, Copyright 2020, with permission from MARCÍLIO ALVES LAJSS.); (c) optimized layout; (d) damage in optimized structure by Amir [68] (Reprinted from Computers & Structures, 114, Amir O, A topology optimization procedure for reinforced concrete structures, 46–58, Copyright 2013, with permission from Elsevier.).

reinforcement layouts yielded by the M-BESO solution were distributed in the damaged areas, which implies that the M-BESO solution can enhance the strength of the corbel. The M-BESO method is an effective optimization method for arranging reinforcements in SRC structures to reduce the tensile stress in concrete.

In this example, both the BESO and M-BESO solutions converged after 125 iterations, as shown in Fig. 11. The compliance and  $R_{FPS > 2}$  for both methods remained relatively stable thereafter. The compliance and  $R_{FPS > 2}$  values for the three structures are listed in Table 2. Compared with the results of the uniform structure, the compliance of the BESO solution decreased by 24.0% and its  $R_{FPS > 2}$  decreased by 18.9%. Compared with the

$R_{FPS > 2}$  of the uniform model and BESO method, the  $R_{FPS > 2}$  of the M-BESO solution decreased by 38.4% and 24.0%, respectively. The FPS contours for structures with different truss layouts are shown in Fig. 12. Compared with the uniform structure, the BESO solution can mitigate the stress concentration significantly but its critical stress area does not change significantly. However, the critical tensile stress region of the M-BESO solution reduced significantly.

#### 4.3 Wall with a window

In this example, a wall with a window, as shown in Fig. 13(a), was analyzed. The wall was under an in-plane

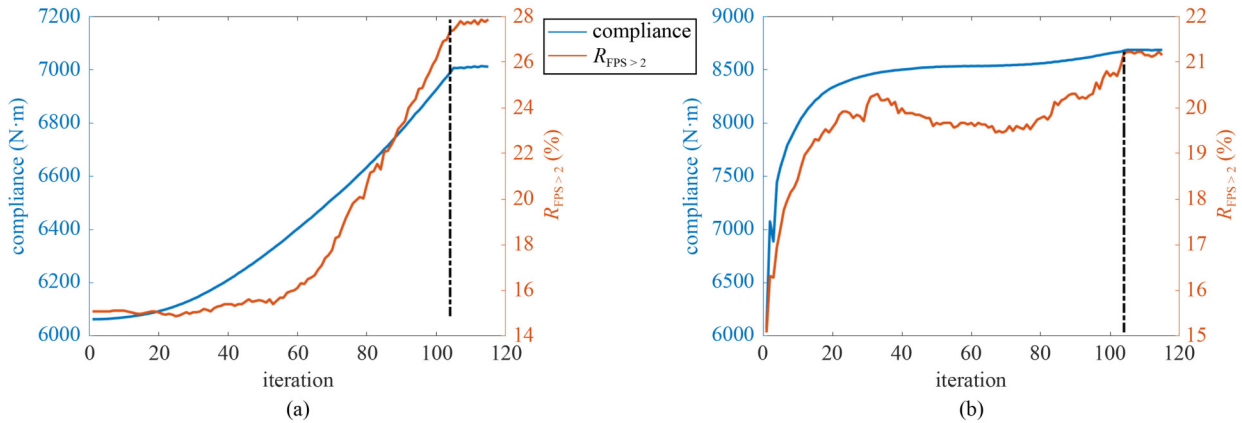


**Fig. 11** Evolutions of compliance and  $R_{\text{FPS} > 2}$  for the corbels: (a) BESO; (b) M-BESO results.

**Table 2** Compliance and  $R_{\text{FPS} > 2}$  for corbels with different truss layouts

indicator	$C$ (N·m)	$R_{\text{FPS} > 2}$ (%)
uniform	9224.5	34.4
BESO	7011.1	27.9
M-BESO	8685.1	21.2

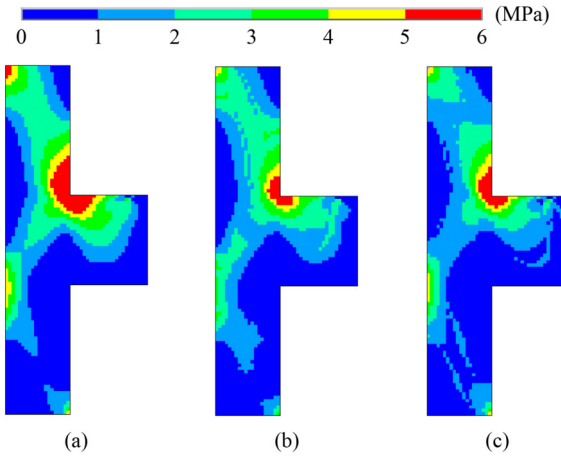


**Fig. 12** FPS contours of the corbels: (a) uniform steel truss; (b) BESO results; (c) M-BESO results.

vertical pressure ( $f$ ) of 800 kN/m along a length of 0.5 m. The left and right ends of the bottom were fixed. The target volume fraction of the steel (truss) elements was  $V_{fs} = 10\%$ , which yielded a reinforcement ratio of 0.68% from the initial over-reinforcement (6.8%). A unit mesh measuring  $0.1 \text{ m} \times 0.1 \text{ m}$  was employed. Thus, the design domain contained 3300 unit hybrid truss-continuum elements.

An SRC structure comprising uniformly distributed steel reinforcing bars with a cross-sectional area of  $7.85 \text{ mm}^2$  was adopted as the benchmark. As illustrated in Fig. 13(b), most of the rebars surrounding the window and the right constraint were under tension. Both layouts obtained via the BESO and M-BESO methods showed clear rebar trajectories, as presented in Figs. 13(c) and

13(d), respectively. The trusses in the BESO solution were arrayed around the window and top-right corner; however, most of the rebars were compressed. The distribution of the steel trusses in the M-BESO solution was completely different from that in the BESO solution. The truss layout in the M-BESO solution was primarily distributed in the top-right corner of the window and the right constraint.

Liang et al. [20] adopted an optimal STM to analyze a wall with a window, as shown in Fig. 14(a), in which the load was rerouted around the opening even when the opening was extremely close to the support. An inclined tensile tie developed across the upper-right corner of the opening, which was susceptible to cracking. The trajectories of the reinforcements obtained using the M-BESO method, as shown in Fig. 13(d), agreed well with the tensile ties in the STM, as shown in Fig. 14(a). Compared with the truss-continuum hybrid material model (Fig. 14(b)) used by Yang et al. [57], the BESO and M-BESO methods can generate more continuous reinforcement designs. The upper-right corner of the opening in the M-BESO solution and the right section of the wall in the BESO solution were similar to those yielded via the damage-based optimization conducted by Amir and Sigmund [54], as shown in Fig. 14(c). In the STM-based design method, the reinforcement was modified by removing unnecessary compressive material (concrete), and rebars were formed only in the tension zone. Silveira et al. [49] designed a detailed reinforcement for a wall with a hole based on an STM, as shown in Fig. 14(d). However, in the M-BESO method based on the truss-continuum hybrid material model, the steel rebars were dispersed in concrete and the original structure remained unchanged. Figure 14(d) shows a practical reinforcement layout redesigned based on an STM [49], which agreed well with the layout of the M-BESO solution. Hence, one can conclude that the proposed method can generate a practical reinforcement layout for SRC structures more efficiently than previous methods.

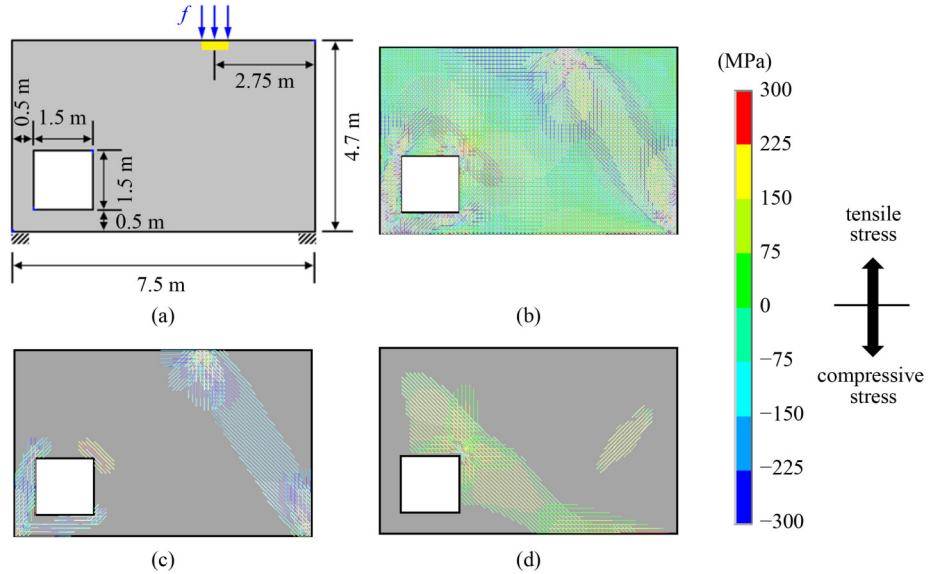


**Fig. 13** Wall with a window: (a) structure; (b) uniform trusses; (c) optimized steel truss layout obtained via BESO; (d) optimized steel truss layout obtained via M-BESO.

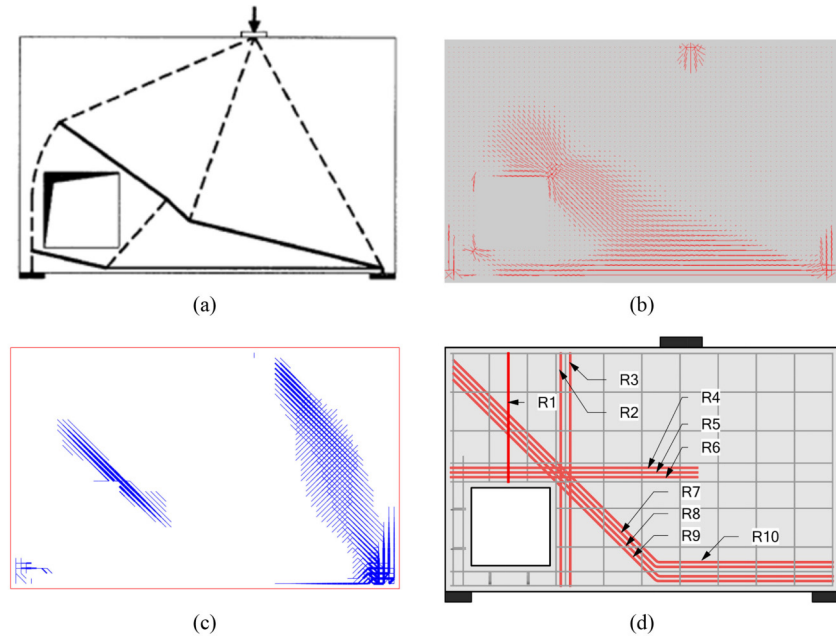


**Fig. 14** Wall with a window: (a) STM from Liang et al. [20] (Authorized reprint from ACI Materials Journal, 97(2), 2000, Liang Q Q, Xie Y M, Steven G P, Topology optimization of strut and-tie models in reinforced concrete structures using an evolutionary procedure.); (b) steel layout from Yang et al. [57] (Reprinted from Structural and Multidisciplinary Optimization, 67(1), Yang Z, Zhou K, Qiao S, Topology optimization of reinforced concrete structure using composite truss-like model, 79–85, Copyright 2018, with permission from Techno.); (c) damage-based topology optimization from Amir and Sigmund [54] (Reprinted from Structural and Multidisciplinary Optimization, 47(2), Amir O, Sigmund O, Reinforcement layout design for concrete structures based on continuum damage and truss topology optimization, 157–174, Copyright 2013, with permission from Springer.); (d) STM-based reinforcement detailing from Silveira et al. [49] (Reprinted from Structures, 41, Silveira M V, Bitencourt L A, Das S, A performance-based optimization framework applied to a classical STM-designed deep beam, 488–500, Copyright 2022, with permission from Elsevier.).

Meanwhile, for the wall with a window, both the BESO and M-BESO solutions converged after 155 iterations, as shown in Fig. 15. The compliance of both methods remained stable when approaching convergence. The  $R_{FPS > 2}$  of the M-BESO solution varied slightly during the

iteration, whereas that of the BESO solution increased rapidly. The compliance values and critical tensile stress area ratios of the three structures are presented in Table 3. Compared with the  $R_{FPS > 2}$  of the uniform structure and BESO solution, the  $R_{FPS > 2}$  of the M-BESO solution

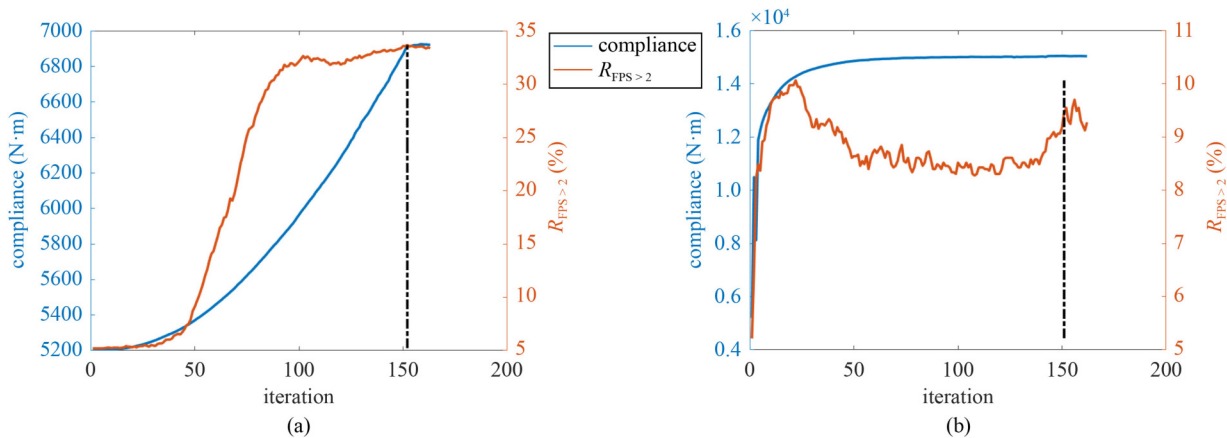


**Fig. 15** Evolution of compliance and  $R_{FPS > 2}$  for wall with a window: (a) BESO; (b) M-BESO results.

decreased significantly by 61.5% and 70.8%, respectively. Based on Fig. 16, the high tensile stress area of the M-BESO solution reduced significantly compared with those of the uniform structure and BESO solution.

**Table 3** Compliance and  $R_{FPS > 2}$  for wall with different truss layouts

indicator	$C$ (N·m)	$R_{FPS > 2}$ (%)
uniform	13045	25.2
BESO	6962	33.2
M-BESO	15036	9.7

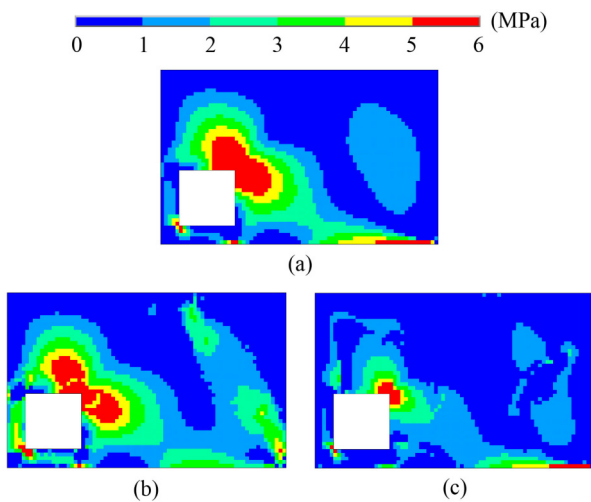


**Fig. 16** FPS contours of wall with a window: (a) uniform steel structure; (b) BESO results; (c) M-BESO results.

## 5 Conclusions

In this study, a BESO-based approach was developed to optimize the layout of steel reinforcements in concrete structures. A hybrid truss-continuum model was developed, where reinforcing steel bars inclined at different angles were considered. Furthermore, a stress-

based modified formulation (M-BESO) was proposed based on the BESO method to control the tensile stresses of the host concrete.

Optimization algorithms that incorporate volume constraints on steel bars were implemented and evaluated based on three numerical examples. For comparison, SRC structures with uniform truss layouts were analyzed. The numerical results showed that both the BESO and M-BESO algorithms yielded clear reinforcement patterns. The conventional BESO solution can yield a truss layout for an SRC structure with high stiffness. Meanwhile, the area of the critical tensile stress in the host concrete yielded by the M-BESO solution was more than 40% lower than those yielded by the uniform layout and the layout from the BESO solution. The M-BESO method effectively improved the stress state of concrete, thereby preventing cracking. In addition, compared with the classical STM-based method, which requires the redesign of the reinforcement layout, the proposed method can directly generate a more practical and reasonable reinforcement layout, which is its most significant advantage.

Using the M-BESO method proposed herein allows the location and direction of reinforcing bars to be optimized simultaneously, thus enabling a reasonable layout of steel reinforcement for concrete structures to be achieved. In addition, because the steel bars are arranged in the tension zone and the concrete in the compression zone endures compressive stress, a lower level of tensile stress can be achieved. This study facilitates the development of a fully digital workflow that can automatically generate efficient steel reinforcements in concrete structures.

**Acknowledgements** This study was supported by the Australian Research Council (FL190100014 and DE200100887).

**Funding note** Open Access funding enabled and organized by CAUL and its Member Institutions.

**Open Access** This article is licensed under a Creative Commons Attribution 4.0 International License (<https://creativecommons.org/licenses/>)

by4.0/), which permits use, sharing, adaptation, distribution and reproduction in any medium or format, as long as you give appropriate credit to the original author(s) and the source, provide a link to the Creative Commons licence, and indicate if changes were made. The images or other third party material in this article are included in the article's Creative Commons licence, unless indicated otherwise in a credit line to the material. If material is not included in the article's Creative Commons licence and your intended use is not permitted by statutory regulation or exceeds the permitted use, you will need to obtain permission directly from the copyright holder. To view a copy of this licence, visit <http://creativecommons.org/licenses/by/4.0/>.

## References

- Shishegaran A, Karami B, Rabczuk T, Shishegaran A, Naghsh M A, Mohammad Khani M. Performance of fixed beam without interacting bars. *Frontiers of Structural and Civil Engineering*, 2020, 14(5): 1180–1195
- Shishegaran A, Varvae H, Rabczuk T, Shishegaran G. High correlated variables creator machine: Prediction of the compressive strength of concrete. *Computers & Structures*, 2021, 247: 106479
- Varae H, Shishegaran A, Ghasemi M R. The life-cycle cost analysis based on probabilistic optimization using a novel algorithm. *Journal of Building Engineering*, 2021, 43: 103032
- Shishegaran A, Boushehri A N, Ismail A F. Gene expression programming for process parameter optimization during ultrafiltration of surfactant wastewater using hydrophilic polyethersulfone membrane. *Journal of Environmental Management*, 2020, 264: 110444
- Es-Haghi M S, Shishegaran A, Rabczuk T. Evaluation of a novel Asymmetric Genetic Algorithm to optimize the structural design of 3D regular and irregular steel frames. *Frontiers of Structural and Civil Engineering*, 2020, 14(5): 1110–1130
- Karami B, Shishegaran A, Taghavizade H, Rabczuk T. Presenting innovative ensemble model for prediction of the load carrying capacity of composite castellated steel beam under fire. *Structures*, 2021, 33: 4031–4052
- Naghsh M A, Shishegaran A, Karami B, Rabczuk T, Shishegaran A, Taghavizadeh H, Moradi M. An innovative model for predicting the displacement and rotation of column-tree moment connection under fire. *Frontiers of Structural and Civil Engineering*, 2021, 15(1): 194–212
- Shishegaran A, Ghasemi M R, Varae H. Performance of a novel bent-up bars system not interacting with concrete. *Frontiers of Structural and Civil Engineering*, 2019, 13(6): 1301–1315
- Shishegaran A, Moradi M, Naghsh M A, Karami B, Shishegaran A. Prediction of the load-carrying capacity of reinforced concrete connections under post-earthquake fire. *Journal of Zhejiang University. Science A*, 2021, 22(6): 441–466
- Bigdely A, Shishegaran A, Naghsh M A, Karami B, Shishegaran A, Alizadeh G. Surrogate models for the prediction of damage in reinforced concrete tunnels under internal water pressure. *Journal of Zhejiang University. Science A*, 2021, 22(8): 632–656
- Abdelaleem T, Diab H M, Rashwan M M. New aspects about the effect of critical regions reinforcement on the strength and moment redistribution of RC continuous T-beams (Experimental and numerical study). *Structures*, 2021, 34: 4834–4850
- Schlaich J, Schafer K. Design and detailing of structural concrete using strut-and-tie models. *Structural Engineering*, 1991, 69: 113–125
- Kumar P. Optimal force transmission in reinforced concrete deep beams. *Computers & Structures*, 1978, 8(2): 223–229
- Biondini F, Bontempi F, Malerba P G. Optimisation of strut and-tie models in reinforced concrete structures. In: Australasian Conference on Structural Optimization. Sydney: Oxbridge Press, 1998, I–10
- Bontempi F, Malerba P G. Stress path adapting strut-and-tie models in cracked and uncracked RC elements. *Structural Engineering and Mechanics*, 2001, 12(6): 685–698
- Ali M A, White R N. Automatic generation of truss model for optimal design of reinforced concrete structures. *ACI Materials Journal*, 2001, 98: 431–442
- Perera R, Vique J. Strut-and-tie modelling of reinforced concrete beams using genetic algorithms optimization. *Construction & Building Materials*, 2009, 23(8): 2914–2925
- Chen A, Cai K, Zhao Z L, Zhou Y, Xia L, Xie Y M. Controlling the maximum first principal stress in topology optimization. *Structural and Multidisciplinary Optimization*, 2021, 63(1): 327–339
- Gao J, Luo Z, Li H, Li P, Gao L. Dynamic multiscale topology optimization for multi-regional micro-structured cellular composites. *Composite Structures*, 2019, 211: 401–417
- Liang Q Q, Xie Y M, Steven G P. Topology optimization of strut-and-tie models in reinforced concrete structures using an evolutionary procedure. *ACI Materials Journal*, 2000, 97: 322–332
- Liang Q Q, Xie Y M, Steven G P. Generating optimal strut-and-tie models in prestressed concrete beams by performance-based optimization. *ACI Materials Journal*, 2001, 98: 226–232
- Leu L J, Huang C W, Chen C S, Liao Y P. Strut-and-tie design methodology for three-dimensional reinforced concrete structures. *Journal of Structural Engineering*, 2006, 132(6): 929–938
- Kwak H G, Noh S H. Determination of strut-and-tie models using evolutionary structural optimization. *Engineering Structures*, 2006, 28(10): 1440–1449
- Brugge M. Generating strut-and-tie patterns for reinforced concrete structures using topology optimization. *Computers & Structures*, 2009, 87(23–24): 1483–1495
- Guan H. Strut-and-tie model of deep beams with web openings—An optimization approach. *Structural Engineering and Mechanics*, 2005, 19(4): 361–380
- He Z Q, Liu Z. Optimal three-dimensional strut-and-tie models for anchorage diaphragms in externally prestressed bridges. *Engineering Structures*, 2010, 32(8): 2057–2064
- Bendsøe M P, Sigmund O. Material interpolation schemes in topology optimization. *Archive of Applied Mechanics*, 1999, 69(9–10): 635–654
- Huang X, Xie Y M. Convergent and mesh-independent solutions for the bi-directional evolutionary structural optimization method. *Finite Elements in Analysis and Design*, 2007, 43(14): 1039–1049
- Da D, Xia L, Li G, Huang X. Evolutionary topology optimization of continuum structures with smooth boundary representation.

- Structural and Multidisciplinary Optimization, 2018, 57(6): 2143–2159
30. Wang M Y, Wang X, Guo D. A level set method for structural topology optimization. Computer Methods in Applied Mechanics and Engineering, 2003, 192(1–2): 227–246
  31. Guo X, Zhang W S, Wang M Y, Wei P. Stress-related topology optimization via level set approach. Computer Methods in Applied Mechanics and Engineering, 2011, 200(47–48): 3439–3452
  32. Wei P, Li Z, Li X, Wang M Y. An 88-line MATLAB code for the parameterized level set method based topology optimization using radial basis functions. Structural and Multidisciplinary Optimization, 2018, 58(2): 831–849
  33. Zhang W, Yuan J, Zhang J, Guo X. A new topology optimization approach based on Moving Morphable Components (MMC) and the ersatz material model. Structural and Multidisciplinary Optimization, 2016, 53(6): 1243–1260
  34. He Z C, Wu Y, Li E. Topology optimization of structure for dynamic properties considering hybrid uncertain parameters. Structural and Multidisciplinary Optimization, 2018, 57(2): 625–638
  35. Zhao Z L, Zhou S, Feng X Q, Xie Y M. Morphological optimization of scorpion telson. Journal of the Mechanics and Physics of Solids, 2020, 135: 103773
  36. Zhao Z L, Zhou S, Feng X Q, Xie Y M. On the internal architecture of emergent plants. Journal of the Mechanics and Physics of Solids, 2018, 119: 224–239
  37. Ma J, Zhao Z L, Lin S, Xie Y M. Topology of leaf veins: Experimental observation and computational morphogenesis. Journal of the Mechanical Behavior of Biomedical Materials, 2021, 123: 104788
  38. Rong Y, Zhao Z L, Feng X Q, Xie Y M. Structural topology optimization with an adaptive design domain. Computer Methods in Applied Mechanics and Engineering, 2022, 389: 114382
  39. Qiu Y, Zhang S, Zhang W, Ye H, Zhang H, Zheng Y. Coupling moving morphable voids and components based topology optimization of hydrogel structures involving large deformation. Journal of Applied Mechanics, 2022, 89(1): 89
  40. Hu Z, Zhang H, Zheng Y, Ye H. Phase-field implicit material point method with the convected particle domain interpolation for brittle–ductile failure transition in geomaterials involving finite deformation. Computer Methods in Applied Mechanics and Engineering, 2022, 390: 114420
  41. Zhao Z L, Zhou S, Cai K, Xie Y M. A direct approach to controlling the topology in structural optimization. Computers & Structures, 2020, 227: 106141
  42. Yang K, Zhao Z L, He Y, Zhou S, Zhou Q, Huang W, Xie Y M. Simple and effective strategies for achieving diverse and competitive structural designs. Extreme Mechanics Letters, 2019, 30: 100481
  43. Ma J, Li Z, Zhao Z L, Xie Y M. Creating novel furniture through topology optimization and advanced manufacturing. Rapid Prototyping Journal, 2021, 27(9): 1749–1758
  44. Xiong Y, Yao S, Zhao Z L, Xie Y M. A new approach to eliminating enclosed voids in topology optimization for additive manufacturing. Additive Manufacturing, 2020, 32: 101006
  45. Xia Y, Langelaar M, Hendriks M A. Optimization-based three-dimensional strut-and-tie model generation for reinforced concrete. Computer-Aided Civil and Infrastructure Engineering, 2021, 36(5): 526–543
  46. Querin O M, Victoria M, Martí P. Topology optimization of truss-like continua with different material properties in tension and compression. Structural and Multidisciplinary Optimization, 2010, 42(1): 25–32
  47. Victoria M, Querin O M, Martí P. Generation of strut-and-tie models by topology design using different material properties in tension and compression. Structural and Multidisciplinary Optimization, 2011, 44(2): 247–258
  48. Liu S, Qiao H. Topology optimization of continuum structures with different tensile and compressive properties in bridge layout design. Structural and Multidisciplinary Optimization, 2011, 43(3): 369–380
  49. Silveira M V, Bitencourt L A, Das S. A performance-based optimization framework applied to a classical STM-designed deep beam. Structures, 2022, 41: 488–500
  50. Yang L, Lin X, Li H, Gravina R J. A new constitutive model for steel fibre reinforced concrete subjected to dynamic loads. Composite Structures, 2019, 221: 110849
  51. Ghasemi H, Kerfriden P, Bordas S P A, Muthu J, Zi G, Rabczuk T. Interfacial shear stress optimization in sandwich beams with polymeric core using non-uniform distribution of reinforcing ingredients. Composite Structures, 2015, 120: 221–230
  52. Guest J K, Moen C D. Reinforced concrete design with topology optimization. In: Structures Congress 2010: 19th Analysis and Computation Specialty Conference. Orlando, FL: American Society of Civil Engineers, 2010, 445–454
  53. Gaynor A T, Guest J K, Moen C. Reinforced concrete force visualization and design using bilinear truss-continuum topology optimization. Journal of Structural Engineering, 2013, 139(4): 607–618
  54. Amir O, Sigmund O. Reinforcement layout design for concrete structures based on continuum damage and truss topology optimization. Structural and Multidisciplinary Optimization, 2013, 47(2): 157–174
  55. Yang Y, Moen C D, Guest J K. Three-dimensional force flow paths and reinforcement design in concrete via stress-dependent truss-continuum topology optimization. Journal of Engineering Mechanics, 2015, 141(1): 04014106
  56. Luo Y, Wang M Y, Zhou M, Deng Z. Optimal topology design of steel–concrete composite structures under stiffness and strength constraints. Computers & Structures, 2012, 112: 433–444
  57. Yang Z, Zhou K, Qiao S. Topology optimization of reinforced concrete structure using composite truss-like model. Structural Engineering and Mechanics, 2018, 67(1): 79–85
  58. Pastore T, Mercuri V, Menna C, Asprone D, Festa P, Auricchio F. Topology optimization of stress-constrained structural elements using risk-factor approach. Computers & Structures, 2019, 224: 106104
  59. Cui H, Zhou K, Yang Z. Reinforcement layout design of RC structures under multiple load cases using truss-like material model. Latin American Journal of Solids and Structures, 2020, 17(4): 17
  60. Ghasemi H, Brighenti R, Zhuang X, Muthu J, Rabczuk T. Optimal

- fiber content and distribution in fiber-reinforced solids using a reliability and NURBS based sequential optimization approach. *Structural and Multidisciplinary Optimization*, 2015, 51(1): 99–112
- 61. Ghasemi H, Brighenti R, Zhuang X, Muthu J, Rabczuk T. Optimization of fiber distribution in fiber reinforced composite by using NURBS functions. *Computational Materials Science*, 2014, 83: 463–473
  - 62. Kwak H G, Filippou F C. Finite Element Analysis of Reinforced Concrete Structures Under Monotonic Loads. Berkeley, CA: Department of Civil Engineering, University of California, 1990
  - 63. Huang X, Xie Y M. Evolutionary Topology Optimization of Continuum Structures: Methods and Applications. Chichester: John Wiley & Sons, 2010
  - 64. Sigmund O, Petersson J. Numerical instabilities in topology optimization: A survey on procedures dealing with checkerboards, mesh-dependencies and local minima. *Structural Optimization*, 1998, 16(1): 68–75
  - 65. Bourdin B. Filters in topology optimization. *International Journal for Numerical Methods in Engineering*, 2001, 50(9): 2143–2158
  - 66. Luo Y, Bao J. A material-field series-expansion method for topology optimization of continuum structures. *Computers & Structures*, 2019, 225: 106122
  - 67. Raphael J M. Tensile strength of concrete. *Proceedings*, 1984, 81: 158–165
  - 68. Amir O. A topology optimization procedure for reinforced concrete structures. *Computers & Structures*, 2013, 114: 46–58